

NASA Technical Memorandum 81576

(NASA-TM-84576) COMPARISON OF MEASURED AND  
CALCULATED MODE REDISTRIBUTION ASSOCIATED  
WITH SPINNING MODE TRANSMISSION THROUGH  
CIRCUMFERENTIALLY SEGMENTED LINED DUCTS  
(NASA) 25 p HC A02/MF A01

N83-26644

Unclas  
03827

CSSL 20A G3/71

# Comparison of Measured and Calculated Mode Redistribution Associated With Spinning Mode Transmission Through Circumferentially Segmented Lined Ducts

Low L. Patton and Willie R. Watson

MARCH 1981

25

1968-1983

NASA

NASA Technical Memorandum 84576

**Comparison of Measured and Calculated  
Mode Redistribution Associated With  
Spinning Mode Transmission Through  
Circumferentially Segmented Lined Ducts**

Tony L. Parrott and Willie R. Watson  
*Langley Research Center  
Hampton, Virginia*

**NASA**

National Aeronautics  
and Space Administration

**Scientific and Technical  
Information Branch**

1983

## SYMBOLS

$A_{m,n}^I, B_{m,n}^I$	incident mode coefficients in hardwall duct sections
$A_{m,n}^\lambda, B_{m,n}^\lambda$	mode coefficients in lined duct sections
$A_{m,n}^\lambda, B_{m,n}^\lambda$	
$A_{m,n}^t, B_{m,n}^t$	transmission mode coefficients in hardwall duct sections
$A_{m,n}^+, A_{m,n}^-$	spinning mode coefficients (clockwise and counterclockwise, respectively) in hardwall duct sections
$c$	free-space sound speed, m/sec
$e$	base for natural logarithm, 2.7183
$f$	frequency, Hz
$J_m(\ )$	mth order Bessel function of first kind
$K_\lambda$	propagation constant associated with $\lambda$ th mode in segmented liner
$k$	free-space wave number
$L$	length of lined duct, m
$m$	circumferential mode number
$m_0$	circumferential mode order of dominant source mode
$N$	normalization constant
$p(r, \theta, z)$	complex acoustic pressure as function of cylindrical coordinates
$p_\lambda(r, \theta)$	eigenmode for circumferentially segmented liner
$R_0$	duct radius, m
$r$	duct radial coordinate
$TL_{m,n}$	power transmission loss for [m,n] mode, dB
$t$	time, sec
$W_m(L)$	transmitted power in mth mode at liner exit
$W_m(0)$	incident power in mth mode at liner entrance
$z$	axial coordinate, m
$\theta$	circumferential coordinate, deg

$\lambda_{m,n}$  hardwall eigenvalues associated with [m,n] mode

$\rho$  density of acoustic medium,  $\text{kg-m}^{-3}$

$Q_{m,n}$  hardwall propagation constant for [m,n] mode

$\omega$  radian frequency,  $2\pi f$ ,  $\text{sec}^{-1}$

Subscripts:

$l$  lined section

$m,n$  circumferential and radial mode order, respectively

## SUMMARY

An experiment was conducted to investigate mode redistribution in lined circular ducts with circumferential impedance nonuniformities. Mode insertion losses were measured for six-segment, two-segment, and uniform liners in a spinning mode synthesizer (SMS) in the quiet flow facility in the Langley Aircraft Noise Reduction Laboratory and correlated with predicted transmission losses.

Both experiment and theory showed that circumferentially segmented duct liners do scatter energy into circumferential modes of different orders. Good agreement between measured and calculated attenuations was obtained for circumferential mode numbers paired with zero order radial mode numbers. When higher order radial modes associated with a given circumferential mode number were cut on, the agreement was not as good.

## INTRODUCTION

There is a continuing need for more efficient duct-liner treatments for the suppression of turbomachinery noise radiated from aircraft engines. In conventional liner design practice, it is generally assumed that equipartition of energy exists among the propagating hardwall duct modes. A uniform admittance liner is then designed to attenuate these modes on the basis of a measured frequency spectrum of the radiated sound. At least two possibilities exist for improving liner performance both of which involve a determination of the source modal spectrum. One possibility is to optimize a uniform liner to attenuate dominant modes. The second possibility is to redistribute the power in the dominant source modes in such a manner that it can be more efficiently attenuated.

Several investigators (refs. 1 to 5) have investigated the possibility of improved liner performance by means of modal redistribution by incorporating circumferential impedance nonuniformities into the liner. A beneficial effect of circumferential liner nonuniformities or segmentation was first reported by Mani (ref. 1). Mani simply blocked off segments of a uniform liner with strips of tape and observed improved performance which he ascribed to mode scattering. Presumably the modal scattering transferred energy into higher order modes which were more rapidly attenuated. If in fact such a mechanism is operative, then exploitation of the concept for practical liner design will require much greater detailed knowledge of the source structure than has heretofore been available. Although analytical studies have predicted the existence of modal redistribution (refs. 2 and 5), there is some difference of opinion regarding the usefulness of circumferential segmentation to achieve liner efficiencies superior to the best uniform liner. Watson (ref. 5) in a parametric study showed that for higher order circumferential modes, a circumferentially segmented liner gives better performance than an optimized uniform liner at the optimal design frequency and even better performance at other frequencies.

In view of potential significant improvements in liner design technology that could ensue from the segmented liner concept, an analytical and experimental program was initiated at the Langley Research Center. The purpose of this paper is to report on the initial phase of the program which was to demonstrate circumferential modal redistribution under controlled laboratory conditions and to compare the results with

analytical predictions. A follow-on experiment will attempt to control mode redistribution in a specified manner by careful control of the wall admittance.

This paper describes an experiment designed to measure modal scattering for circumferentially segmented test liners consisting of two and six segments. Baseline data for a uniform impedance test liner are also presented. Results for measured and predicted modal attenuations for incident, standing circumferential modes of orders 1 and 3 are presented.

### THEORY

The theoretical results presented in this paper are based on a lengthy analysis which is developed in detail elsewhere (ref. 5). In this section only the underlying assumptions and an outline of the analysis are given.

Figure 1 shows a schematic of the duct liner configuration under consideration. An incident sound field on the source side of the liner can be described as a superposition of hardwall modes as follows at the liner/hardwall interface:

$$p(r, \theta, z) = \sum_{m=0}^{\infty} \sum_{n=0}^{\infty} \left( A_{m,n}^I \cos m\theta + B_{m,n}^I \sin m\theta \right) \frac{J_m(\lambda_{m,n} r)}{N_{m,n}} e^{iQ_{m,n} z} \quad (1)$$

where

$$N_{m,n}^2 = \int_0^{2\pi} \int_0^{R_0} J_m^2(\lambda_{m,n} r) \cos^2 m\theta r dr d\theta \quad (2)$$

and

$\lambda_{m,n}$  hardwall eigenvalues

$Q_{m,n}$  axial propagation constant for hardwall duct

$A_{m,n}^I, B_{m,n}^I$  incident mode coefficients

$z, \theta, r$  axial, circumferential, and duct radial coordinate, respectively

$J_m(\ )$  mth order Bessel function

Similarly, the transmitted sound on the termination side of the liner is expressed as a superposition of hardwall modes:

$$p(r, \theta, z) = \sum_{m=0}^{\infty} \sum_{n=0}^{\infty} \left( A_{m,n}^t \cos m\theta + B_{m,n}^t \sin m\theta \right) \frac{J_m(\lambda_{m,n} r)}{N_{m,n}} e^{iQ_{m,n} z} \quad (3)$$

where  $A_{m,n}^t$  and  $B_{m,n}^t$  are transmission mode coefficients; the sound field in the circumferentially segmented liner is expressed in terms of the characteristic functions  $p_\ell(r, \theta)$  for the segmented liner:

$$p(r, \theta, z) = \sum_{\ell=0}^{\infty} \left( A^\ell e^{iK_\ell z} + B^\ell e^{-iK_\ell(z-L)} \right) p_\ell(r, \theta) \quad (4)$$

where

$A^\ell, B^\ell$  mode coefficients

$K_\ell$  propagation constant

$L$  length of lined duct

$p_\ell(r, \theta)$  eigenmode for circumferentially segmented liner

As shown in reference 5, the hardwall duct modes can be used as basis functions for expanding the characteristic functions for the segmented liner:

$$p_\ell(r, \theta) = \sum_{m=0}^{\infty} \sum_{n=0}^{\infty} \left( A_{m,n}^\ell \cos m\theta + B_{m,n}^\ell \sin m\theta \right) J_m(\lambda_{m,n} r) \quad (5)$$

where  $A_{m,n}^\ell$  and  $B_{m,n}^\ell$  are mode coefficients. Galerkin's method is employed to obtain the coefficients in equatio. (5) as well as the axial propagation constant  $K_\ell$  for the segmented liner. This modal expansion (eq. (4)) is then matched to the hard-wall modes at the appropriate interface to determine the reflected sound  $p^R$  on the source side of the liner as well as the hardwall coefficients  $A_{m,n}^t$  and  $B_{m,n}^t$  on the termination side of the liner. The insertion losses for the  $[m,n]$  mode are

$$TL_{m,n} = 10 \log_{10} \left[ \frac{\left( \left| A_{m_o,n}^I \right|^2 + \left| B_{m_o,n}^I \right|^2 \right) \operatorname{Re} \left( Q_{m_o,n} \right)}{\left( \left| A_{m,n}^t \right|^2 + \left| B_{m,n}^t \right|^2 \right) \operatorname{Re} \left( Q_{m,n} \right)} \right] \quad (6)$$

In this paper, predicted and experimentally determined values of  $TL_{m,n}$  are compared to determine if both the experiment and theory show circumferential mode scattering. Such a comparison is also employed to determine the validity of the theory.

#### EXPERIMENTAL TEST SETUP

The experimental setup for performing this experiment is depicted schematically in figure 2. The spinning mode synthesizer (SMS) in the quiet flow facility in the

Langley Aircraft Noise Reduction Laboratory consists of 24 compression drivers equally spaced around the circumference of the hardwall source section as shown. By adjusting amplitude and phase for each driver a desired mode can be generated with an isolation of about 20 dB. Desired test modes were set up and optimized by means of existing computer codes on the basis of phase and amplitude information sensed at the 48 microphones located at equal circumferential intervals at the source plane as illustrated in the figure. The optimizing procedure involved comparing the desired and actual pressure distribution at the source plane and making systematic adjustments to the driver inputs to minimize an optimization parameter in a multidimensional space. Further details of the SMS operation are described in reference 6. The synthesized sound field is propagated through the test liner into another hardwall section and finally terminated by an open-celled foam wedge to minimize reflections. The inside diameter of the duct system was 0.30 m (11.79 in.) throughout.

The modal content of the incident and transmitted sound field was inferred by a pressure-field mapping rig located between the test section and the nonreflecting termination as depicted in figure 2. The mapping rig consisted of two radially traversing microphones spaced 0.0635 m (2.5 in.) apart installed on a rotating section of the duct. The mechanical positioning and data acquisition were implemented under computer control.

The modes incident on the lined test section were inferred from measurements with the lined test section replaced by a hardwall duct. To validate the assumption that the source output remained invariant with modest changes in source loading, the termination was modified to produce significant reflections over the frequency range of interest. No significant change in the dominant mode content of the source was observed for this change. It was therefore assumed that the lined test section would cause no significant change in the source output. On this basis, measured modal insertion losses for the lined test section were equated to the modal transmission losses.

#### INSTRUMENTATION

A block diagram of the automated instrumentation system used for data acquisition is shown in figure 3. A complete description of this system and its performance is given in reference 6. A brief description of the system is given here.

The traversing microphone probes are installed in a rotatable section of the hardwall duct as illustrated in figure 2. The radial coordinates and number of equally spaced azimuthal positions of the probes are input at the computer terminal as part of the test plan. The prescribed field positions for the probes are then located automatically by means of a sequence of commands from the computer to stepping motors that control probe radial and azimuthal positions. The existing acoustic field is sampled and the resulting data are multiplexed into the computer with appropriate signal conditioning. The data are then scaled by using stored phase and amplitude calibration information and presented graphically on a cathode ray tube at the computer terminal and also stored on disk file for further analysis. Temperature was continuously monitored in the test duct and input to the data file at the start of a data acquisition sequence.

## DATA ANALYSIS

The pressure-field mapping data described previously were processed to yield the modal composition of the sound field in the hardwall duct sections. The mathematical procedure for this modal decomposition procedure is described in detail in reference 6 and is outlined here. The pressure at any location in the duct can be described as follows:

$$\sum_{m=-\infty}^{\infty} \sum_{n=0}^{\infty} \left( A_{m,n}^+ e^{iQ_{m,n}^+ z} + A_{m,n}^- e^{iQ_{m,n}^- z} \right) J_m(\lambda_{m,n} r) e^{i(m\theta - \omega t)} = p(r, \theta, z) \quad (7)$$

The indices  $m$  and  $n$  represent the azimuthal wave number and radial mode number, respectively; the superscripts (+ and -) on the mode amplitude coefficients indicate the direction of travel for axially propagating waves;  $J_m$  is the Bessel function of the first kind and order  $m$ ; and  $\lambda_{m,n}$  represents hardwall eigenvalues. The axial propagation constant is given by

$$Q_{m,n}^{\pm} = \pm(k^2 - \lambda_{m,n}^2)^{1/2} \quad (8)$$

where  $k = \omega/c$  is the free-space wave number. The mode amplitude coefficients  $A_{m,n}^+$  and  $A_{m,n}^-$  are to be determined.

The modal decomposition is obtained by performing a Fourier decomposition in the coordinate  $\theta$  and a Bessel decomposition in the coordinate  $r$  on each of two sets of pressure-field data. For example, the field data at axial location  $z_1$  would be transformed as follows:

$$\int_0^{2\pi} \int_0^{R_0} p(r, \theta, z_1) e^{-im\theta} J_m(\lambda_{m,n} r) r dr d\theta = p(m, n, z_1) \quad (9)$$

With the orthogonality properties of the complex exponential and Bessel functions, a set of algebraic equations can be written in terms of the transformed data as follows:

$$A_{m,n}^+ e^{iQ_{m,n}^+ z_1} + A_{m,n}^- e^{iQ_{m,n}^- z_1} = p(m, n, z_1) \quad (10)$$

$$A_{m,n}^+ e^{iQ_{m,n}^+ z_2} + A_{m,n}^- e^{iQ_{m,n}^- z_2} = p(m, n, z_2) \quad (11)$$

Resolution of the pressure field into  $m$  azimuthal wave numbers requires  $2m$  equi-spaced azimuthal pressure measurements at each radial position. To include up to  $n = 9$  radial modes in the analysis, 10 radial pressure measurements were taken and fitted with a cubic spline routine. Generally, enough azimuthal locations were used to insure that all propagating modes were incorporated into the analysis.

The theoretical analysis was based upon the standing mode representation given by equations (1) and (3). It was necessary to transform the measured spinning mode coefficients  $A_{m,n}^+$  and  $A_{m,n}^-$  to the appropriate standing mode coefficients  $A_{m,n}$  and  $B_{m,n}$  in order to compare experimental and theoretical results. This transformation is given by

$$\frac{A_{m,n}}{N_{m,n}} = \left( A_{+m,n}^+ + A_{+m,n}^- \right) + (-1)^m \left( A_{-m,n}^+ + A_{-m,n}^- \right) \quad (12)$$

$$\frac{B_{m,n}}{N_{m,n}} = \left( A_{+m,n}^+ + A_{+m,n}^- \right) - (-1)^m \left( A_{-m,n}^+ + A_{-m,n}^- \right) \quad (13)$$

Since only positive-going modes were of interest in this experiment, the above equations reduce to

$$\frac{A_{m,n}}{N_{m,n}} = A_{+m,n}^+ + (-1)^m A_{-m,n}^+ \quad (14)$$

$$\frac{B_{m,n}}{N_{m,n}} = A_{+m,n}^+ - (-1)^m A_{-m,n}^+ \quad (15)$$

Note that the positive and negative spinning modes are indicated explicitly.

#### TEST LINER CONFIGURATIONS

Test liner configurations were obtained by arranging six liner elements, each of which occupied  $60^\circ$  of duct circumference, in a test duct casing as shown in figure 4. The axial length of each liner element was 0.222 m (8.75 in.) and consisted of perforated face sheet bonded to phenolic honeycomb of thickness 0.0254 m (1.0 in.). Two different face-sheet porosities were used to achieve the nonuniformity in circumferential impedance. A complete test configuration consisted of two casings joined such that axially adjacent liner elements were aligned with respect to their impedance properties. In this manner, a circumferentially segmented test liner configuration was built with an active axial length of 0.444 m (17.5 in.) and an inside diameter of 0.30 m (11.79 in.). A uniform impedance liner test configuration with the same geometry as the nonuniform impedance liner was also fabricated for baseline comparisons. The impedance for this liner was chosen equal to the greater of the two impedances

used for the nonuniform liner. A third impedance test liner configuration was achieved by blocking a 180° circumferential segment of the uniform liner with tape.

#### TEST LINER IMPEDANCES

Target impedances for the test liner elements were constrained by existing hardware geometry, available face-sheet materials with predictable acoustic properties, and desired impedance behavior over the frequency range of interest. Three other considerations influenced the choice of liner impedances. Firstly, it was thought desirable to have the impedance discontinuity between liner elements invariant with frequency because it was not known a priori at which frequencies significant modal redistribution could be observed. Secondly, it was desirable to stay well away from optimum modal impedances to avoid wiping out redistributed modes. Thirdly, since impedances in the neighborhood of  $10\rho c$  or greater reflect better than 98 percent of the incident energy, it would be just as appropriate to use a hardwall to implement target impedances of this magnitude. In view of these considerations, several liner element samples were fabricated for impedance measurements in a standing wave impedance tube.

Impedance measurements for the two liner elements selected for the circumferentially segmented liner fabrication are shown in figure 5. Two sets of measurements are shown in this figure. The open symbols represent the measured impedances for the two selected liner elements for a constant sound pressure level (SPL) of 100 dB at the sample face. The solid symbols are the measured impedances for an SPL of 125 dB at the sample face. As can be observed, the resistance ratio difference is relatively constant over the entire frequency range even though the liner elements exhibit significant nonlinearity with increasing SPL. Since the incident dominant mode amplitude levels in the SMS were typically 125 to 130 dB, the impedance values corresponding to the higher levels were used in the theoretical calculations. The backing depths for the test liner elements were chosen to be 0.0127 m (0.5 in.). In combination with the perforated face sheets, this backing depth produced measured reactances shown in figure 5(b). Clearly, nonlinear effects are not nearly so pronounced for the reactances as for resistances. The tuning frequency (zero reactance) is seen to be about 1.2 kHz for both test liner elements.

#### SELECTION OF SOURCE MODES

Prior to installation of the test liner configurations in the test setup, a series of hardwall test modes were selected and optimized for maximum isolation from contaminating modes on SMS. The driver amplitude and phase settings were then stored in a data file for later recall. The ranges of relevant test modes and driving frequencies were jointly determined by the limitations of the SMS facility and theoretical guidance in regard to expected modal redistribution for a given mode incident upon the test duct configuration. For the test duct configurations fabricated for this experiment, azimuthal mode numbers of 0, 1, 3, and 4 were selected. Attempts were made to optimize these modes at several different frequencies. Since SMS does not control the radial mode content, increasing the driving frequency incorporates an increasing number of higher order radial modes into the test mode setup corresponding to a given azimuthal mode content. Figure 6 shows an eigenmode parametric plot for the hardwall duct system used in this experiment. The plot shows azimuthal mode number  $m$  plotted against nondimensional cut-on frequency  $kR_0$  with the radial mode number  $n$  as a parameter. The vertical lines on the plot indicate the selected frequencies at which azimuthal mode numbers 1 and 3 were optimized. Note that for a

given azimuthal mode number, more radial mode orders become cut on as the driving frequency is increased. The results achieved with azimuthal mode numbers 1 and 3 for driving  $kR_0$  values of 4.5, 5.5, and 7.8 are discussed in the section "Results and Discussion" as typical of the many test modes investigated.

#### ANALYSIS OF SOURCE MODES

The availability of only one reliable mode decomposition station in the duct test setup as shown in figure 2 mandated that comparisons of theoretical and measured results be accomplished by correlating measured mode insertion losses with calculated mode transmission losses for the test duct configurations. If, in fact, the modal structure of the source output (i.e., positive-going modes from the source incident upon the test duct section) does not change with changes in source loading (e.g., changes in the test duct configuration), then mode transmission losses and mode insertion losses can be equated. To check the validity of this assumption for this experiment, the termination was modified to produce significant reflections (most likely more than would be produced by changing the duct test section). The results of this check suggested that the dominant mode was essentially invariant with significant changes in the reflectivity of the termination. However, significant changes in the relative phases of the subdominant modes were observed. This behavior was not deemed to be of great importance because mode redistribution was expected to be controlled by the dominant incident mode which generally carried in excess of 95 percent of the total energy.

#### RESULTS AND DISCUSSION

To provide perspective, the results of this experiment are presented in two different formats. The first format will show a comparison of incident and transmitted spinning mode pressure amplitudes as obtained directly from the data analysis program. The data are presented for all three test duct configurations (i.e., uniform, six-segment, and two-segment liners) for three different dominant incident modes. No comparison with theoretical prediction is presented in this format. The second format shows a comparison between theory and experiment in terms of modal power transmission losses through the test duct configuration. In the theoretical calculations, however, only the dominant mode is allowed as input to the test duct. Power redistributed into other spinning modes is then expressed as follows:

$$TL_m = 10 \log \left( \frac{W_{m_0}(0)}{W_m(L)} \right) \quad (16)$$

Here,  $W_{m_0}(0)$  represents the incident power in the dominant mode  $m_0$  and  $W_m(L)$  represents the transmitted power in the  $m$ th mode. Thus,  $TL_m$  represents the amount of incident power that is redistributed and then absorbed from circumferential mode  $m_0$  to circumferential mode  $m$  and then transmitted through the duct.

Figure 7 represents typical measured incident and transmitted modal pressure amplitude levels for the three test liner configurations investigated in this experiment. The mode levels are plotted over a range of 40 dB with the 0-dB level arbitrarily referenced to that of the dominant incident mode level shown in parentheses.

The test liners are represented by the region bounded by vertical lines with identifying labels. The incident and transmitted modes are represented as propagating from left to right and are indexed appropriately. Since all mode levels were referenced to that of the dominant mode, the transmitted mode levels can be considered as modal transmission losses under the assumption discussed in the section "Analysis of Source Modes." Isolations of the dominant, incident modes are shown in figure 7 to range from 15 to 22 dB. This level of isolation implies that the dominant mode carried greater than 95 percent of the incident power and was judged adequate for observing significant modal scattering. The upper limit on modal isolations achieved in this experiment is a kind of system dynamic range determined jointly by SMS and the data acquisition system. Typical contributors to the mode isolation noise floor are random calibration errors, random probe positioning errors, and electronic noise. Therefore in view of the foregoing remarks, only data from 0 to -20 dB in figure 7 are taken as quantitatively meaningful. However, mode levels from -20 to -40 dB are shown in the belief that collective trends may be meaningful in a qualitative sense.

The data presented in figure 7(a) represent a mode, [1,0], driven well above its cut-on frequency (see fig. 6); figure 7(b) represents a higher order radial mode, [1,1], driven just above its cut-on frequency; figure 7(c) represents a mode, [3,0], driven well above its cut-on frequency. For all cases, the only measurable, significant mode redistribution occurs for the two-segment test liner. There is a hint that some scattering may be occurring for the [2,0] mode for the six-segment liner driven by the [1,0] mode at  $kR_0 = 4.5$  and for the mode [5,0] and [1,0] when driven by the dominant mode [3,0] at  $kR_0 = 7.8$ ; however, these levels are on the threshold of violating the signal/noise ratio criterion discussed previously. For the two-segment test liner, significant modal redistributions are seen to occur into the [2,0] mode when driven by dominant mode [1,0] at  $kR_0 = 4.5$  and into the [1,0], [2,0], and [4,0] modes when driven by dominant mode [3,0] at  $kR_0 = 7.8$ . This case offers reliable evidence for mode scattering since all the significantly scattered modes are within 17 dB of the transmitted dominant mode. Note however that for the two-segment liner driven by dominant mode [1,1] at  $kR_0 = 5.5$  there was no measurable scattering.

A comparison of measured and calculated spinning mode attenuations for the uniform and two-segment test liner configurations is shown in figure 8. Results are shown for each of the two test liner configurations for three different incident modes. The  $[m,n]$  values for the incident modes are [1,0], [1,1], and [3,0] driven at the respective  $kR_0$  values of 4.5, 5.5, and 7.8. As in figure 7, all transmitted mode levels are referenced to the incident mode level so that the figures present comparisons of measured and calculated mode transmission losses directly. A comparison of measured and calculated transmission losses for the uniform liner test configuration is shown in figure 8(a). For this test configuration excellent agreement is obtained between experiment and theory when all higher order radial modes are included in the comparison for a given circumferential m-number. This test provided a baseline comparison for the experimental test procedure and theoretical prediction scheme. The excellent agreement between theory and experiment for this case suggests that the experimental and computational procedures are fundamentally sound. Note also that there is no evidence of energy redistribution into other circumferential modes on the transmission side of the duct as would be expected for a uniform liner.

Shown in figure 8(b) are comparisons of measured and calculated individual  $[m,n]$  modal attenuations relative to the incident mode level for the two-segment test liner configuration. Both experiment and theory show significant circumferential mode redistribution for  $kR_0 = 4.5$  and  $kR_0 = 7.8$  whereas no significant redistribution occurs for  $kR_0 = 5.5$ . Such consistency of trends is very encouraging. For the test

case corresponding to a  $kR_0$  value of 5.5, the measured mode levels were more than 20 dB down from the incident mode level which exceeds the dynamic range criterion for the measurement/analysis procedure as discussed previously. For the two test cases in which mode redistribution is evident, the measured and calculated mode levels are in good agreement provided that no higher order radial modes are cut on. If, however, higher order radial modes are cut on for a given circumferential m-number, then discrepancies are observed. In particular, for the test case corresponding to a  $kR_0$  value of 4.5 there is a discrepancy between the measured and calculated mode levels for the [0,0] mode in which case the [0,1] mode is cut on at the  $kR_0$  value of 3.8. (See fig. 6.) For the test case corresponding to the  $kR_0$  value of 7.8, there is a significant discrepancy between measured and calculated mode levels for the [1,0] mode in which case the [1,1] mode is cut on at a  $kR_0$  value of 5.3. Also the discrepancy between measured and calculated mode levels for the [2,0] modes correlates with the observation that the [2,1] mode becomes cut on at a  $kR_0$  value of 6.7. The consistency of these results suggest that the details of mode redistributions may be highly sensitive to series truncation (eqs. (3) to (5)) which can change the mode amplitude coefficients that represent the pressure distributions in the hard and soft wall sections. In addition, from the experimental standpoint, liner inhomogeneities and nonlinearities as well as incident modal phasing relative to the circumferential liner segment orientation may have a greater effect when higher order radial modes are propagating.

#### CONCLUSIONS

The results of this research support the following conclusions:

- (1) Both the experimental data and analytical model show that circumferentially segmented duct liners do redistribute acoustic energy into circumferential modes of different orders.
- (2) The measured and calculated attenuations for individual [m,n] modes are in excellent agreement when no higher order radial modes are cut on for a given circumferential m-number.
- (3) Instances of discrepancies between measured and calculated mode attenuations for a given [m,n] mode are observed to correlate with the cut on state of higher order radial modes for a particular circumferential m-number.

In general the results of this effort are very encouraging. Confidence in the analytical model has been established which can be used to further evaluate mode redistributions as a means of designing superior sound absorbing duct liners.

Langley Research Center  
National Aeronautics and Space Administration  
Hampton, VA 23665  
February 11, 1983

#### REFERENCES

1. Mani, Ramani: Acoustic Duct With Peripherally Segmented Acoustic Treatment. U.S. Pat. 3,937,590, Feb. 10, 1976.
2. Namba, M.; and Fukushige, K.: Application of the Equivalent Surface Source Method to the Acoustics of Duct Systems With Non-Uniform Wall Impedance. J. Sound & Vib., vol. 73, no. 1, Nov. 8, 1980, pp. 125-146.
3. Astley, R. J.; Walkington, N. J.; and Eversman, W.: Transmission in Flow Ducts With Peripherally Varying Linings. AIAA-80-1015, June 1980.
4. Watson, Willie R.: Noise Suppression Characteristics of Peripherally Segmented Duct Liners. NASA TP-1904, 1981.
5. Watson, Willie R.: Circumferentially Segmented Duct Liners Optimized for Axisymmetric and Standing-Wave Sources. NASA TP-2075, 1982.
6. Silcox, Richard J.; and Lester, Harold C.: Sound Propagation Through a Variable Area Duct: Experiment and Theory. AIAA-81-1967, Oct. 1981.

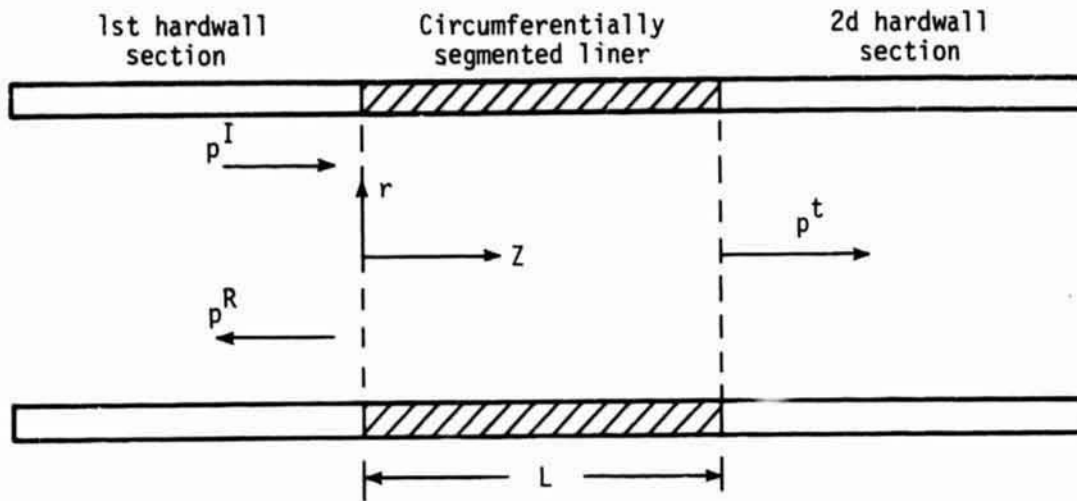


Figure 1.- Configuration employed to develop mode matching equations.

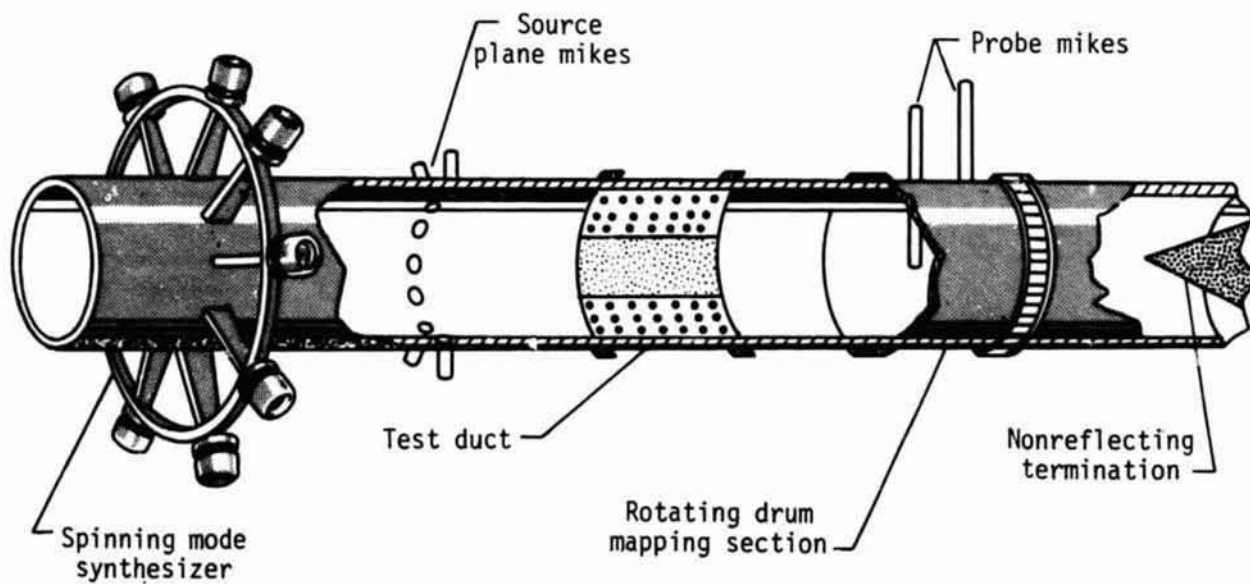


Figure 2.- Schematic of experimental setup.

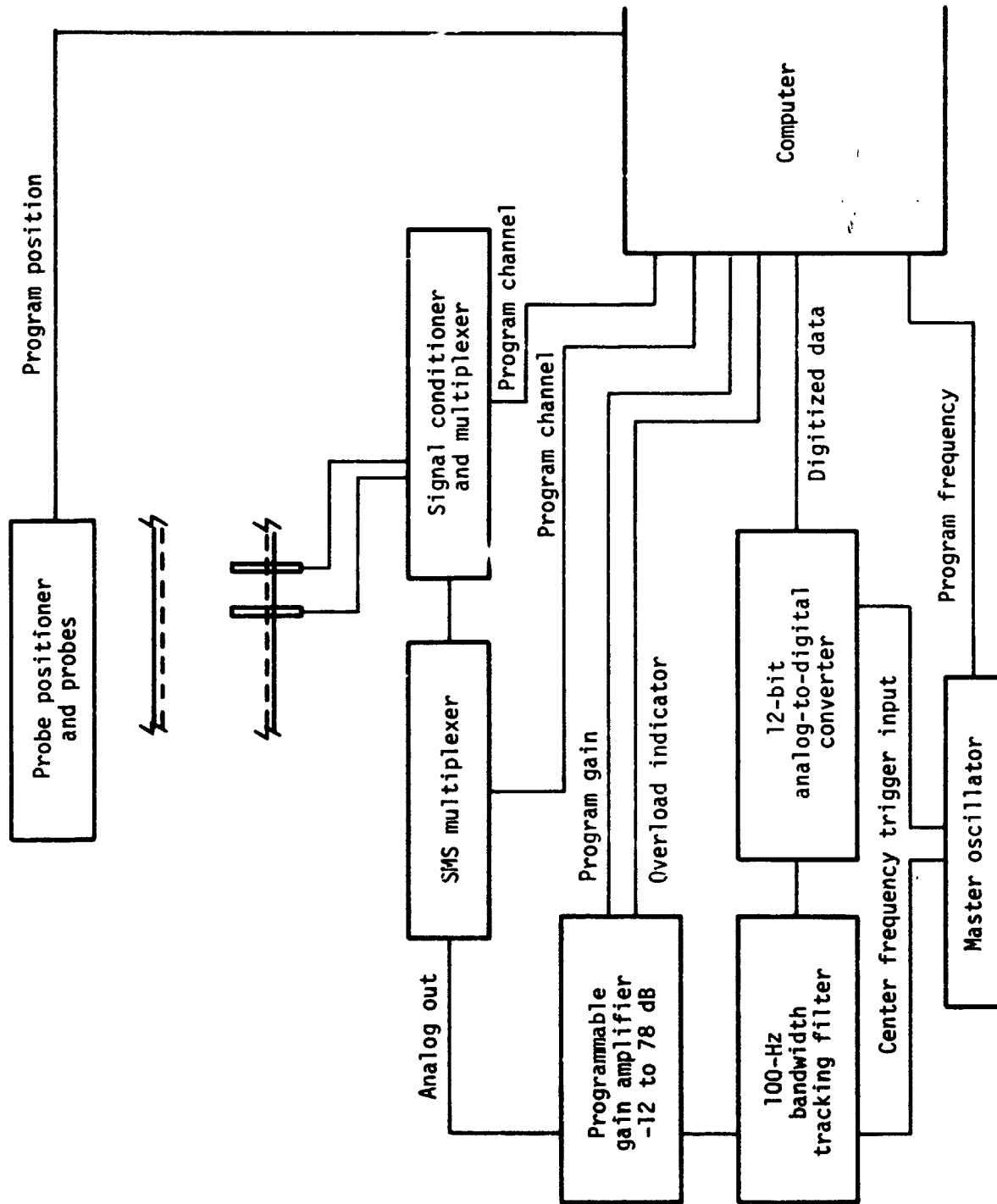
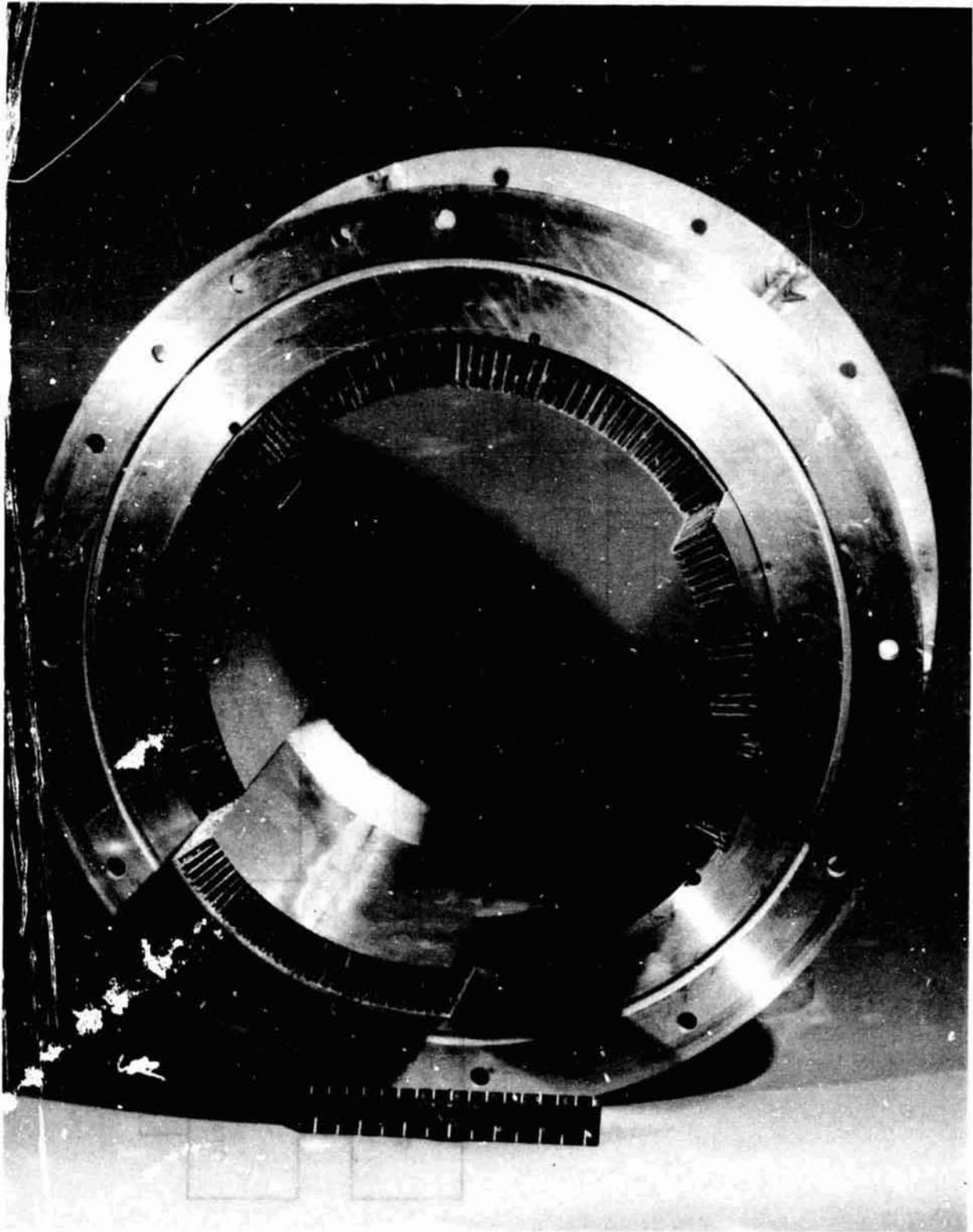
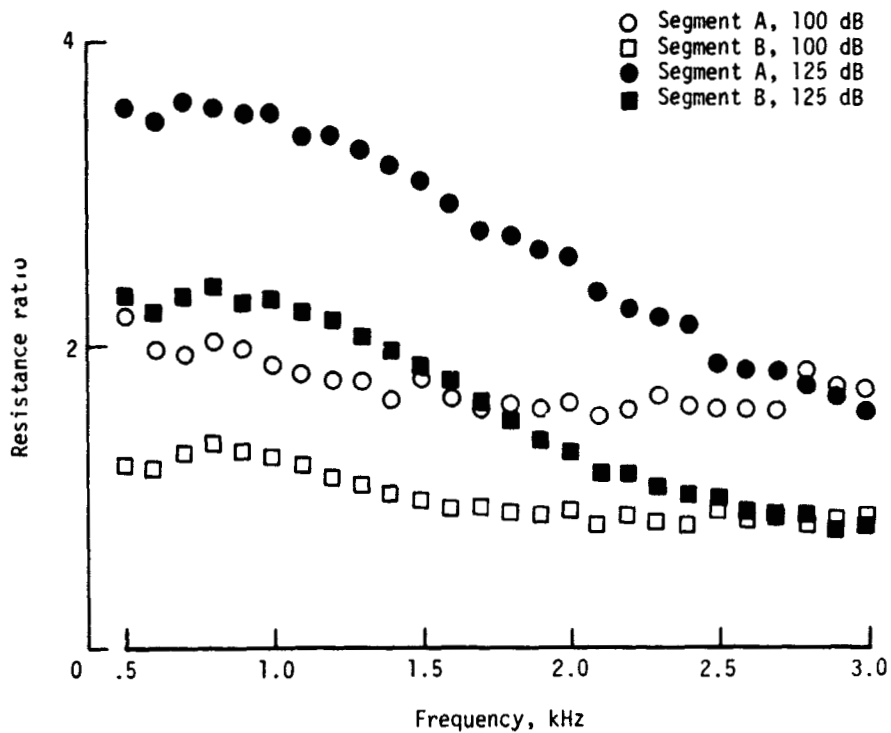


Figure 3.- Automated instrumentation for data acquisition.

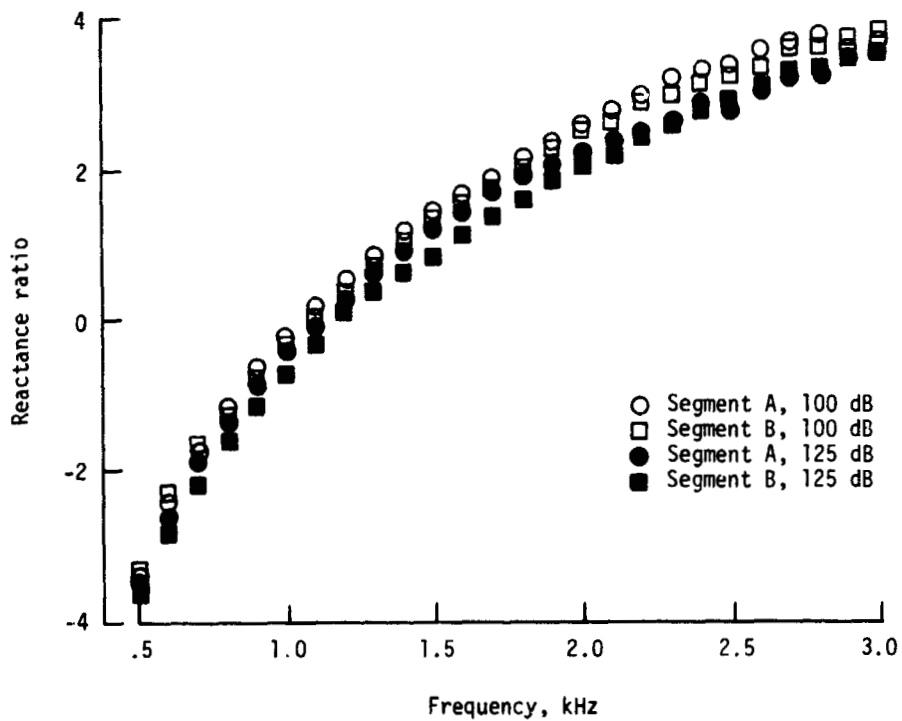


L-82-6498

Figure 4.- Test duct casing showing installation of 60° test liner elements.



(a) Resistance ratio.



(b) Reactance ratio.

Figure 5.- Measured impedance of test liner elements.

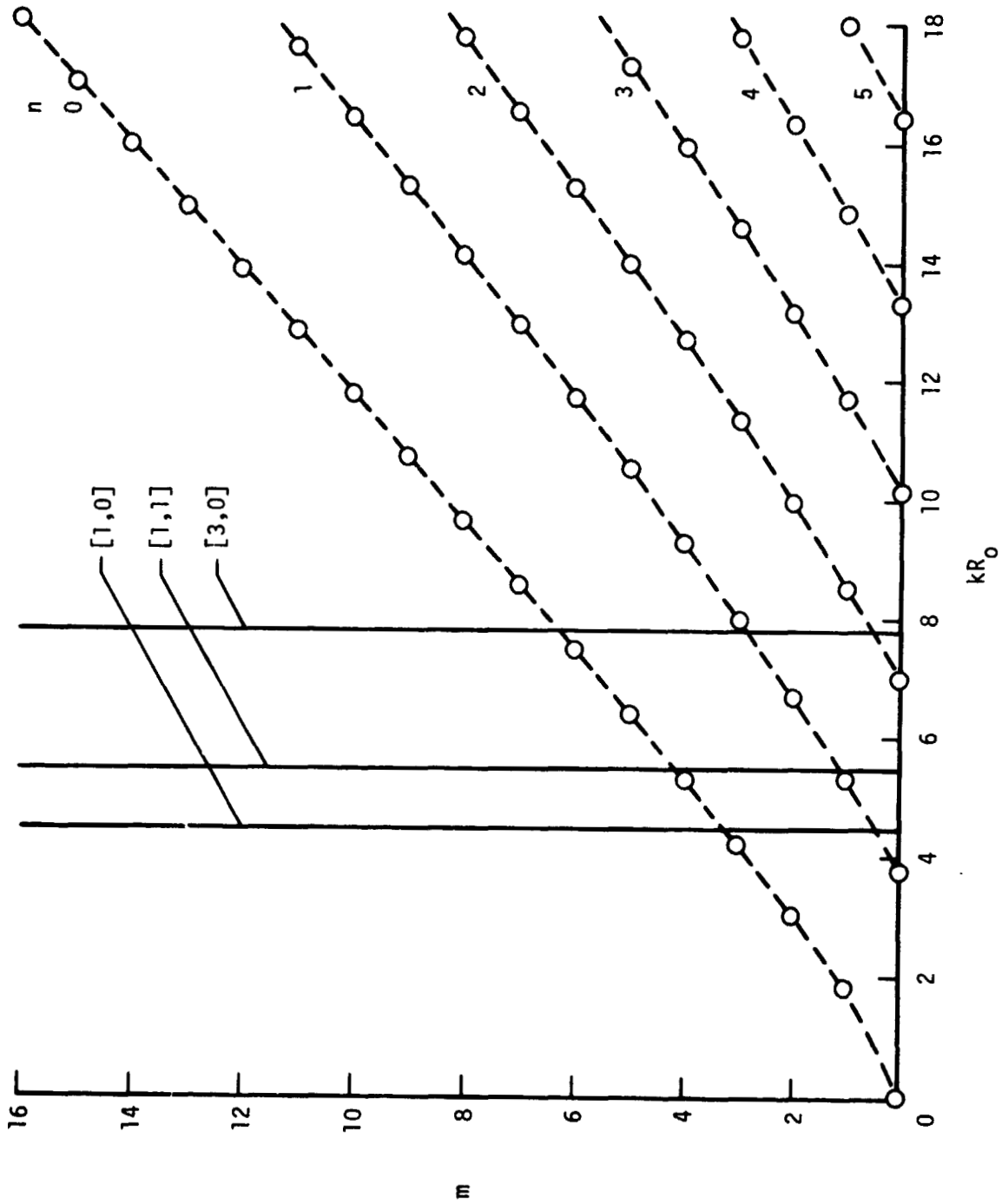
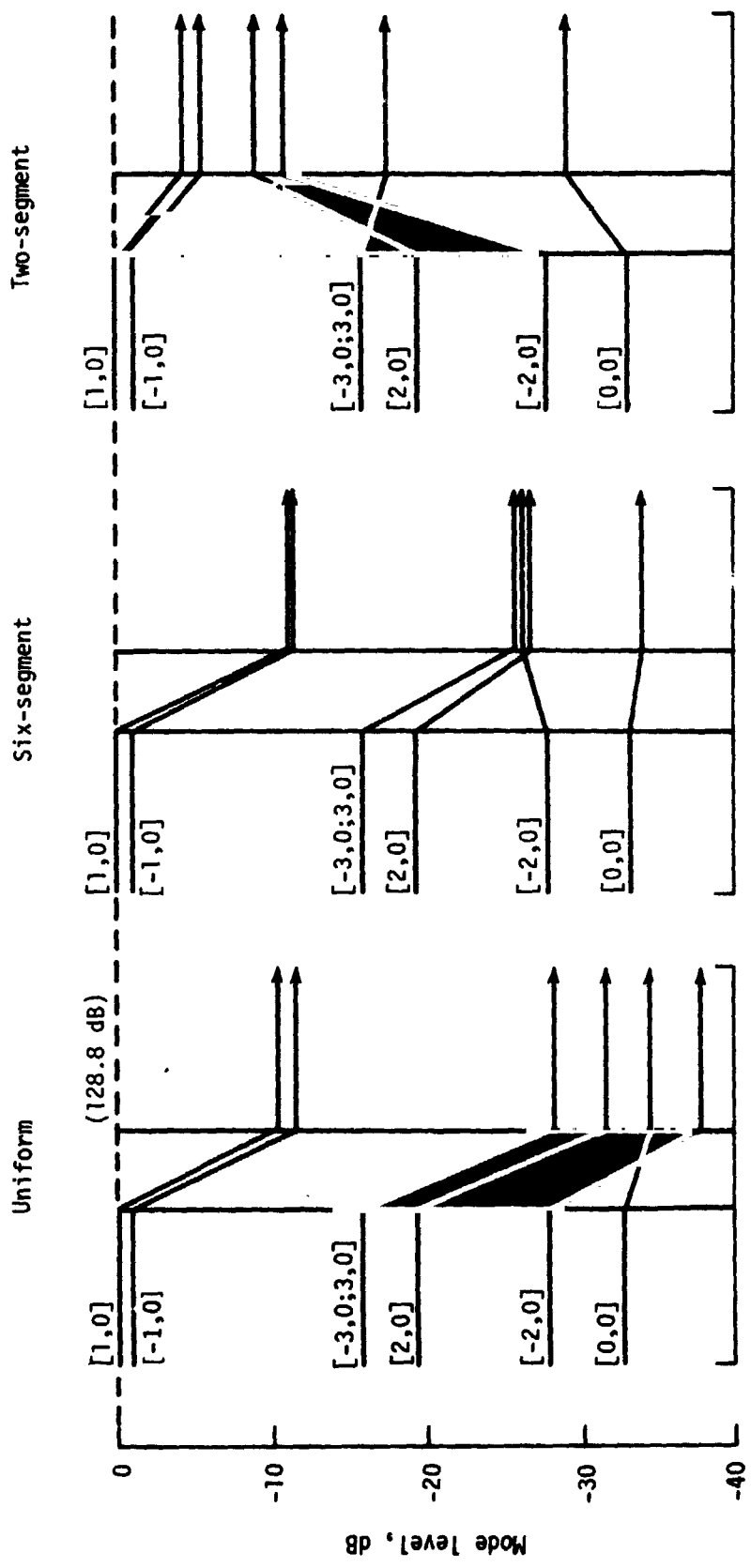
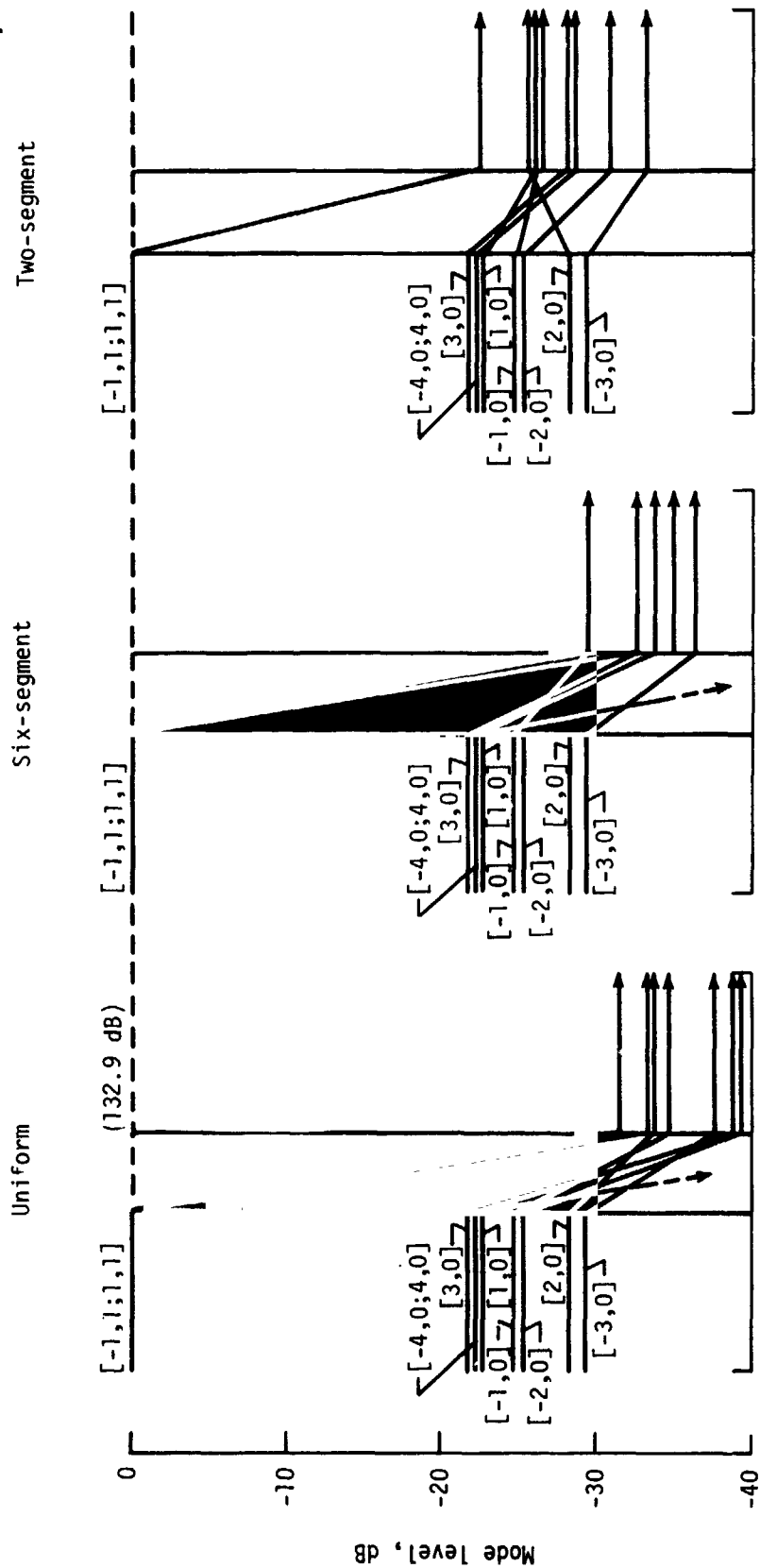


Figure 6.- Parametric plot of mode cut-on frequencies showing  $kR_0$  values at which dominant modes were driven.



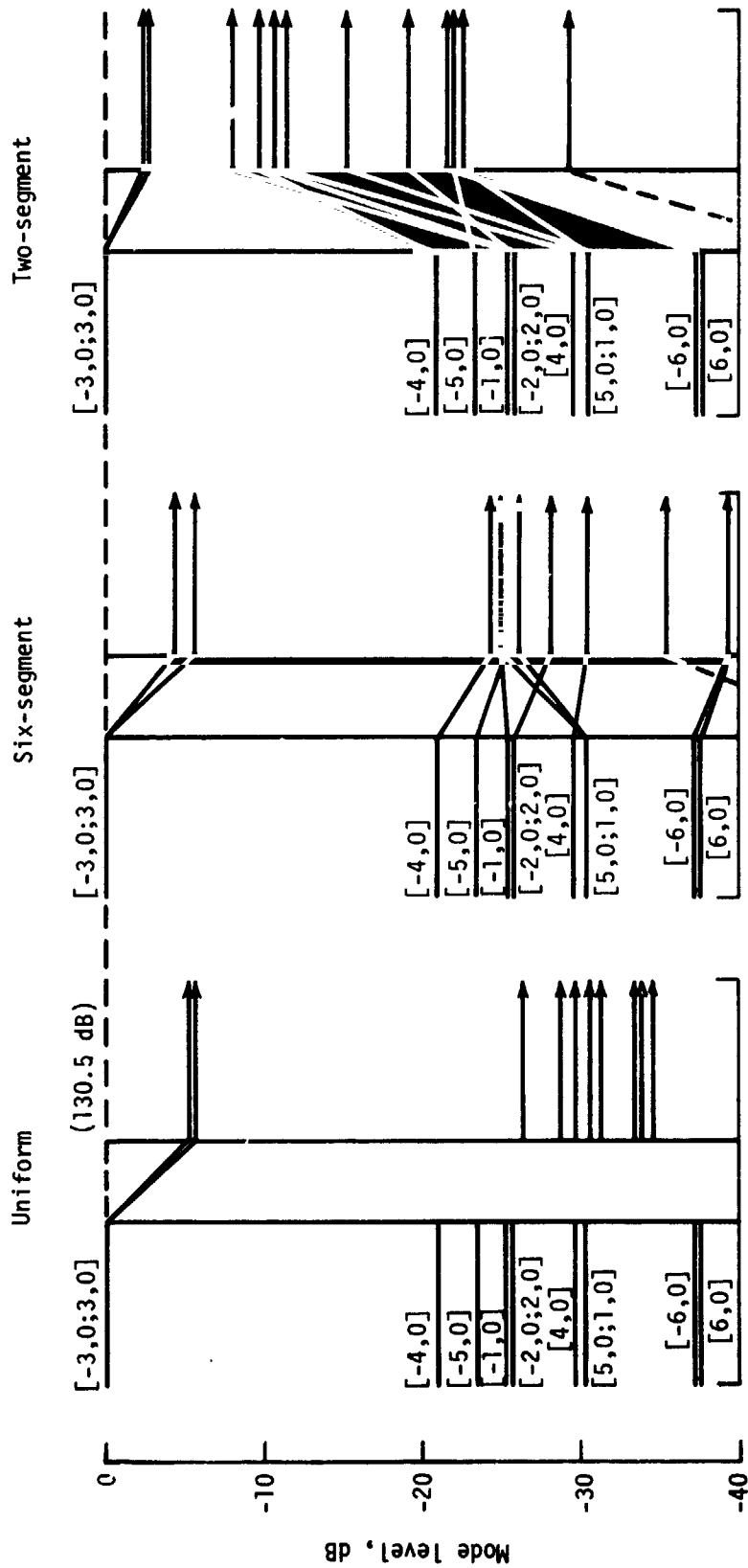
(a)  $kR_0 = 4.5$ .

Figure 7.- Incident and transmitted modes.



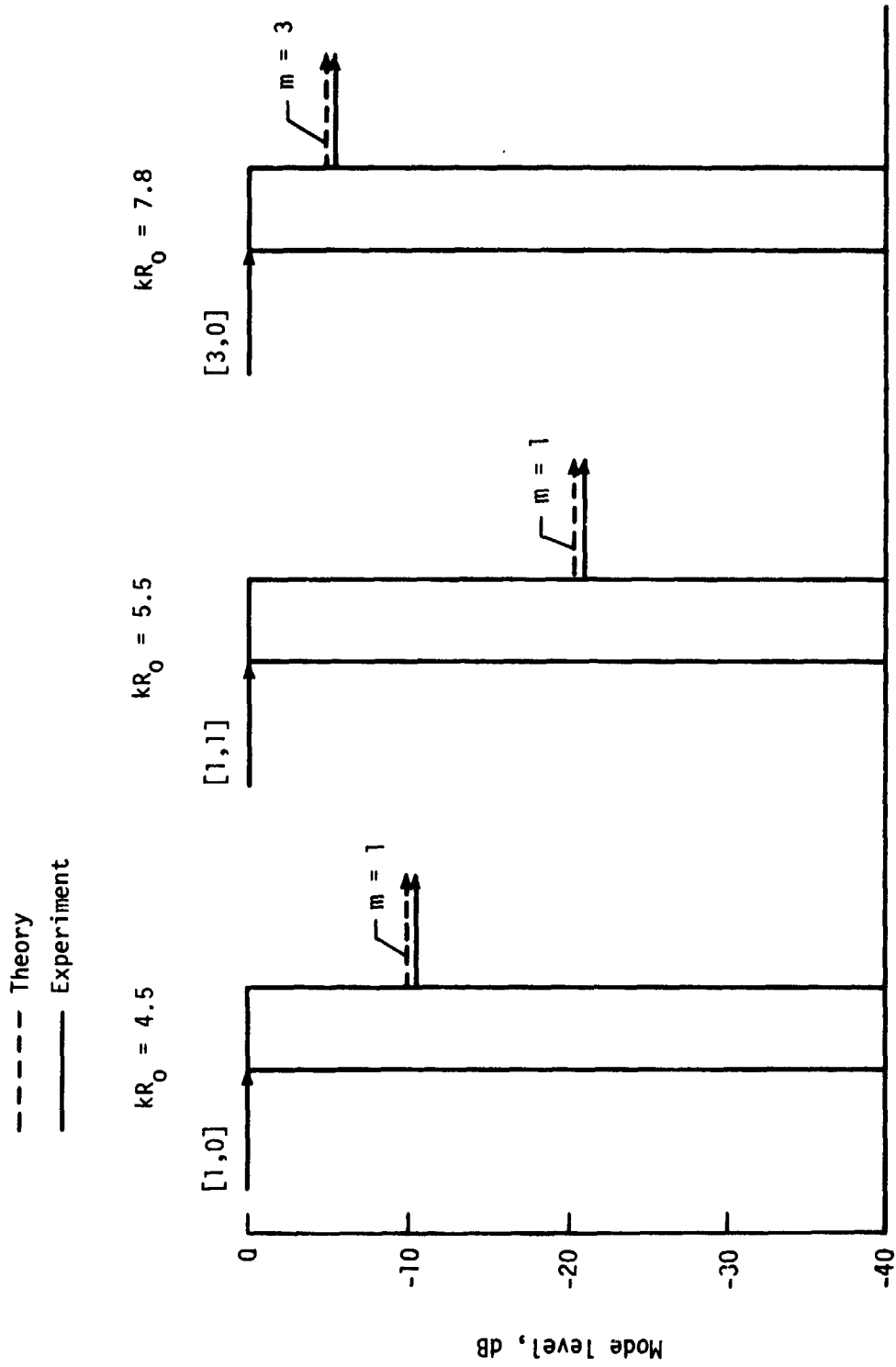
(b)  $kR_0 = 5.5$ .

Figure 7.- Continued.



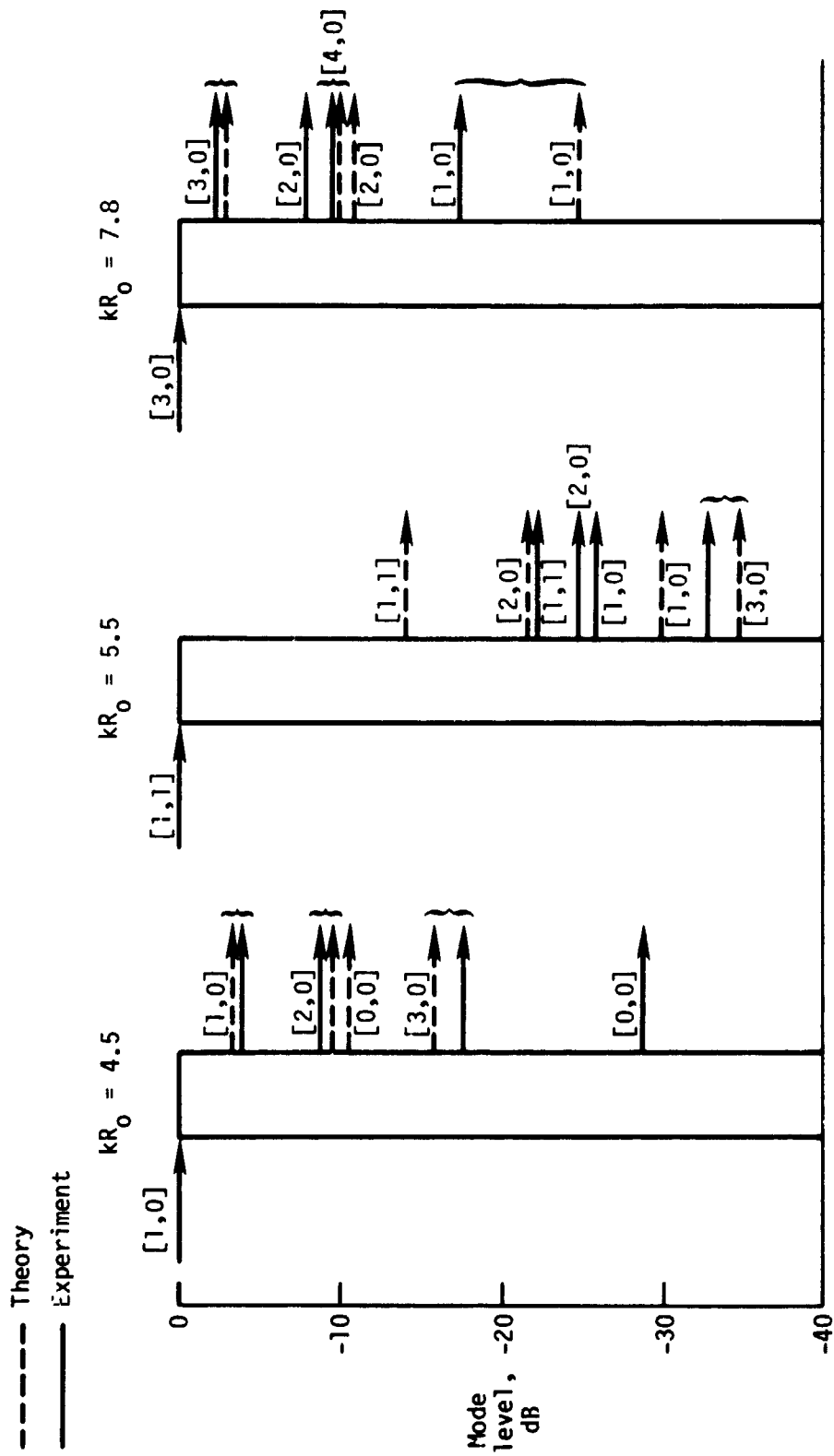
(c)  $kR_0 = 7.8$ .

Figure 7.- Concluded.



(a) mth order spinning mode for uniform liner.

Figure 8.-- Comparison of experimental and predicted levels.



(b)  $[m,n]$  spinning mode for segmented liner.

Figure 8.- Concluded.

1. Report No. NASA TM-84576		2. Government Accession No.		3. Recipient's Catalog No.	
4. Title and Subtitle COMPARISON OF MEASURED AND CALCULATED MODE REDISTRIBUTION ASSOCIATED WITH SPINNING MODE TRANSMISSION THROUGH CIRCUMFERENTIALLY SEGMENTED LINED DUCTS				5. Report Date March 1983	
				6. Performing Organization Code 505-31-33-13	
7. Author(s) Tony L. Parrott and Willie R. Watson				8. Performing Organization Report No. L-15548	
9. Performing Organization Name and Address NASA Langley Research Center Hampton, VA 23665				10. Work Unit No.	
				11. Contract or Grant No.	
12. Sponsoring Agency Name and Address National Aeronautics and Space Administration Washington, DC 20546				13. Type of Report and Period Covered Technical Memorandum	
				14. Sponsoring Agency Code	
15. Supplementary Notes					
16. Abstract  An experiment was conducted to investigate mode redistribution in lined circular ducts with circumferential impedance nonuniformities. Mode insertion losses were measured for six-segment, two-segment, and uniform liners in a spinning mode synthesizer (SMS) in the quiet flow facility in the Langley Aircraft Noise Reduction Laboratory and correlated with predicted transmission losses. Both experiment and theory showed that circumferentially segmented duct liners do scatter energy into circumferential modes of different orders. Good agreement between measured and calculated attenuations was obtained for circumferential mode numbers paired with zero order radial mode numbers. For the higher order radials, the agreement was not as good.					
17. Key Words (Suggested by Author(s)) Mode scattering Impedance nonuniformities Mode coupling Peripheral segmentation Duct propagation				18. Distribution Statement Unclassified - Unlimited  Subject Category 71	
19. Security Classif. (of this report) Unclassified		20. Security Classif. (of this page) Unclassified		21. No. of Pages 24	22. Price A02